Atmospheric simulations using Venus AORI general circulation models

M. Yamamoto (RIAM, Kyushu Univ.), K. Ikeda & M. Takahashi (NIES)

#AORI: *Atmosphere and ocean Research Institute, Univ. Tokyo.*

This work is supported by cooperative research project for climate system research of **AORI**.

T63L52 with radiative transfer and topography

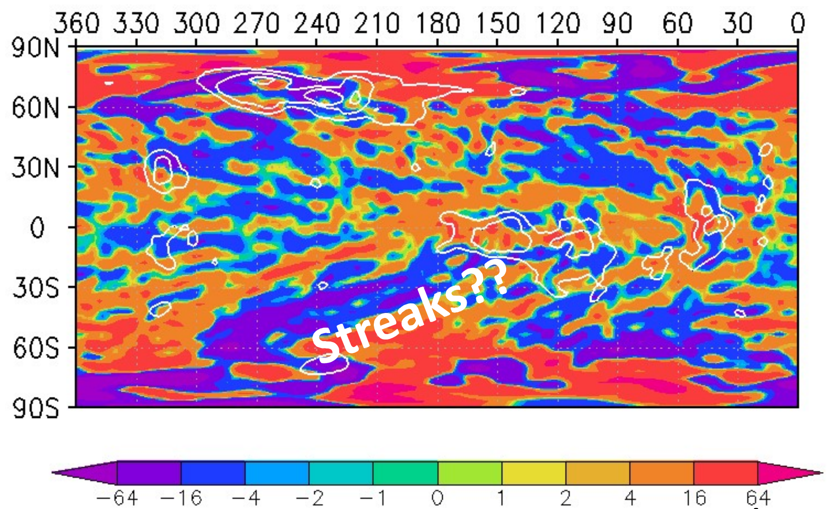

Snapshot of vertical flow (mm/s) at 50 km ~ *cloud base*

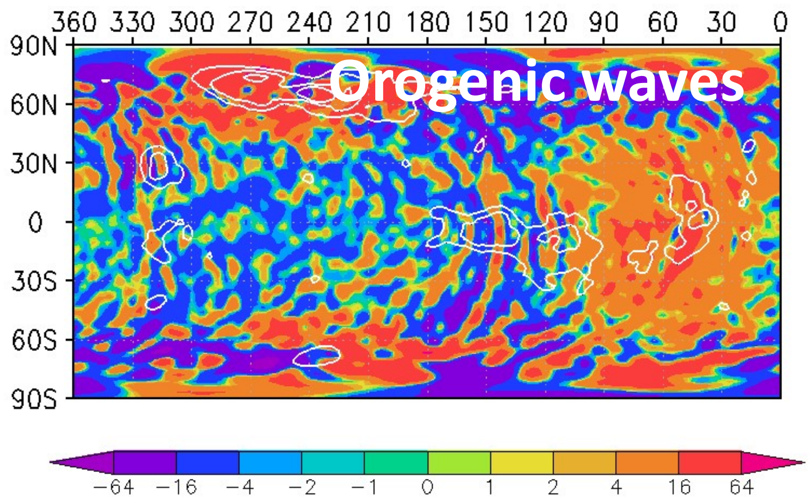

Snapshot of vertical flow (mm/s) at 60 km ~ *upper clouds*

Overview of Venus AORI GCM

1. Venus GCM with simplified radiation

Venus GCM from initially motionless state

Yamamoto & Takahashi (2003JAS) : SR by zonal mean heating (T10)

Yamamoto & Takahashi (2003GRL) : SR by zonal mean heating (T21), fast Kelvin wave

Yamamoto & Takahashi (2004GRL, 2006JAS, 2009JGR) : SR by 3D heating, thermal tide, & Kelvin-Rossby waves

Yamamoto & Takahashi (2007EPS) : SR by 3D heating with topography

Yamamoto & Takahashi (2007GRL, 2008AA) : Effects of seasonal variation & planetary rot.

Venus middle atmospheric GCM

Yamamoto & Takahashi (2012Icarus) : Dynamics of Kelvin wave

Yamamoto & Takahashi (2015PSS) : Polar vortex in the presence of thermal tide

Yamamoto & Takahashi (2018Icarus) : Interannual zonal-flow variation

Sensitive issues for dynamical core in extremely long-term time integrations

Yamamoto & Takahashi (2016, 2018JGR) : Effects of planetary rot. & horizontal res. (T21to106)

Our recent work : Sensitivity to horizontal subgrid-scale (SGS) diffusion (T42)

2. Venus GCM with radiative transfer

Ikeda (2011PhD) : developments of radiation code and gravity wave parameterization

Kuroda, U. Tohoku group et al. : application to cloud model

Yamamoto et al (2019Icarus) : T21 with topography and radiative code

Our recent work : T63 with topography and radiative code

Sensitivity of dynamical core to horiz. SGS diffusion

4th-order, 6hr for max. n | 4th-order 24hr for max. n | 4th-order, 120hr for max. n | 6th-order, 720hr for max. n

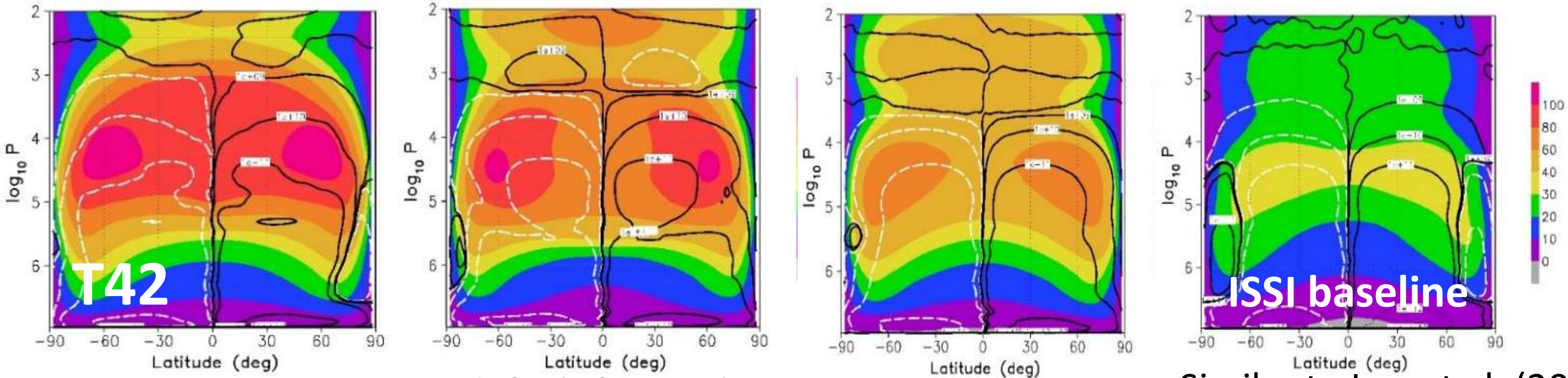

default for Earth

Similar to Lee et al. (2007)

➡ SR depends on the horiz. SGS diffusion in extremely long-term experiments from initially motionless for ISSI baseline run

VGCM with topography and radiative code

< Purpose >

To accurately simulate thermal tides, stationary waves and general circulation by a realistic Venus GCM, along with fine and large cloud features.

➡ The results shows following slides of our presentation

Model (Ikeda 2011 PhD)

1. Dynamical core : CCSR/NIES/FRCGC AGCM ver.5.6
   T21L52, T63L52 (Numaguti et al. 1997)

2. Radiative transfer : Discrete-Ordinate/Adding, 2-stream
   (Nakajima et al. 2000)
   - IR and Solar: 28 bands
   - Gas absorption
     - Correlated k-distribution method
     - CO_2: CDSD-1000, sub-Lorentz lineshape(Fukabori et al., 1986)
     - H_2O, SO_2, OCS, CO: HITRAN2004, Voigt lineshape
     - Collision-induced absorption by CO_2 (Moskalencko et al., 1979)
   - Cloud
     - 75% H_2SO_4 (refractive index: Palmer and Williams, 1975)
     - log-normal 3 mode (Pollack et al., 1980)
     - Unknown UV absorber (Crisp, 1986)

3. Gravity-wave momentum parameterization is not used.

4. Magellan topography height data (Ford & Pettengill 1992)

#The details of model setup in Yamamoto et al. (2019 Icarus, 321, 232-250).

Model setup

Temperature

Initial: VIRA (Seiff et al. 1985)

Zonal wind

Nudging run <u>until equilibrium</u>

0－10Vdays: U is nudged to Uref with a time constant of 3 Edays.

10－90Vdays: Zonal-mean component of U below 40 km is nudged to Uref with a time const. of 3 Edays.

Nudging-free run <u>after equilibrium</u>

90－93Vdays⇒*Data analysis*

Reference zonal flow Uref

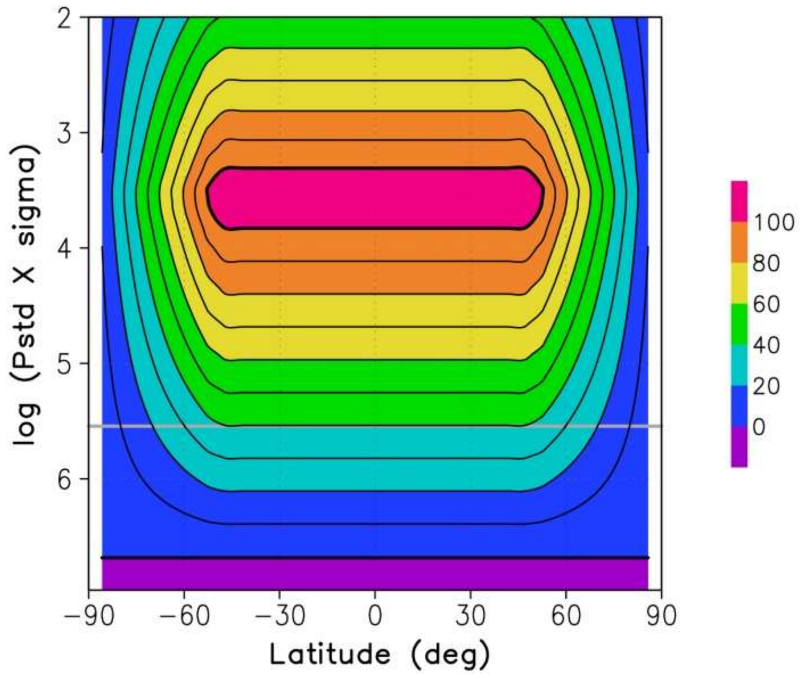

Topography

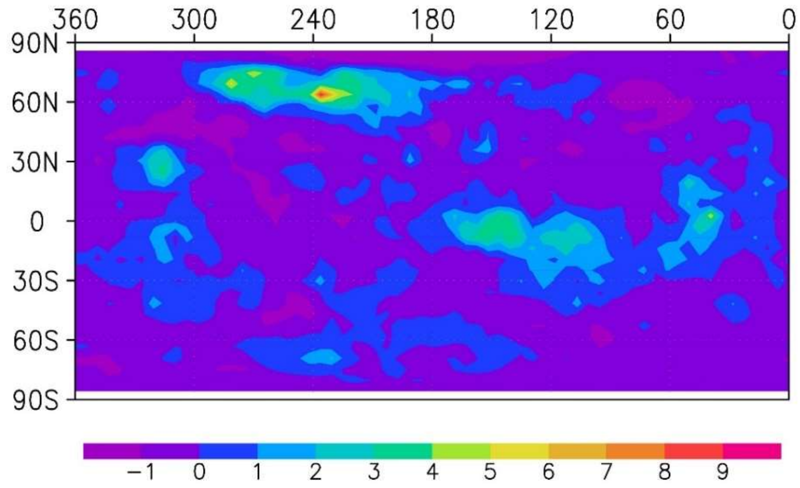

T21 Nudging run

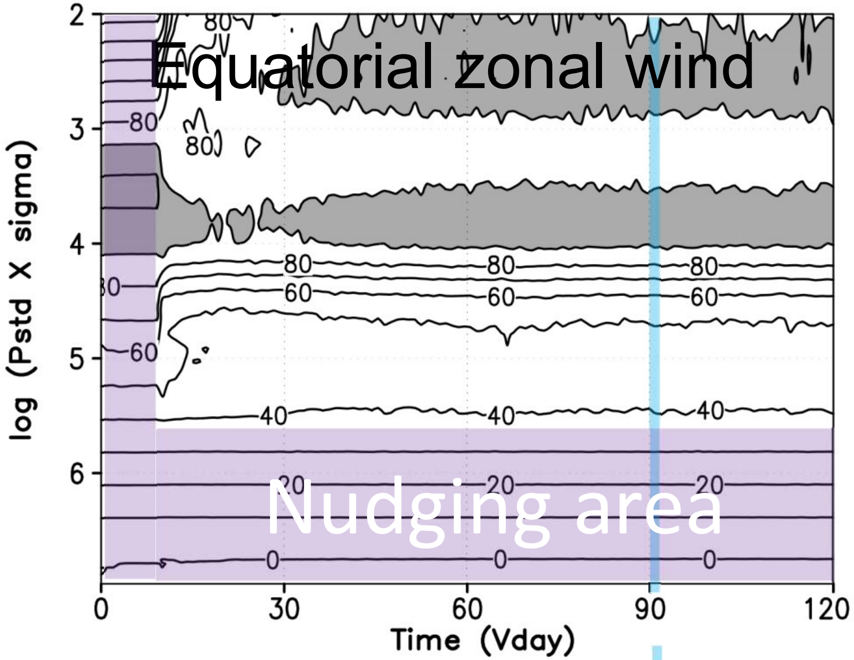

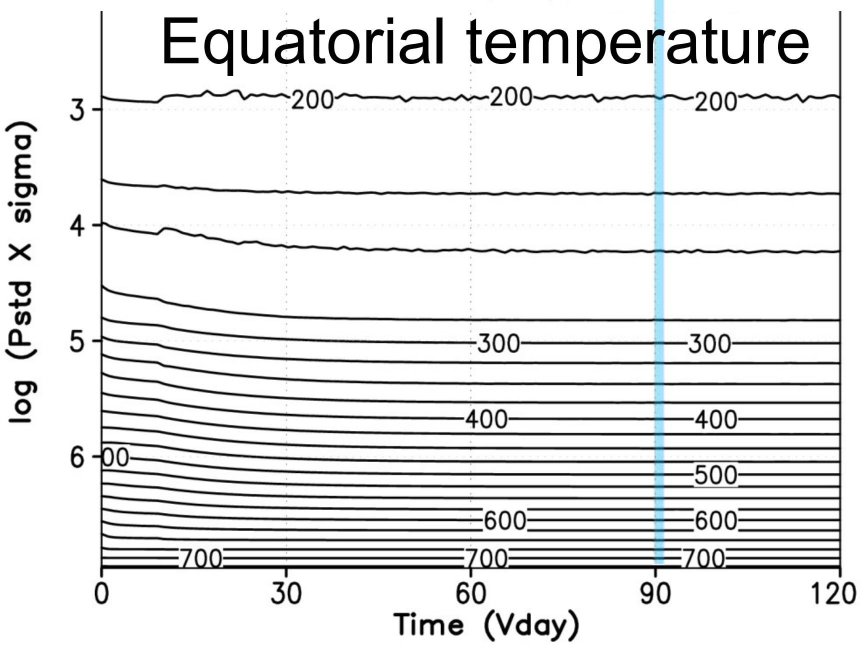

T63 Nudging-free run

We analyzed the nudging-free model output

Zonal-mean equatorial flow of nudging-free run

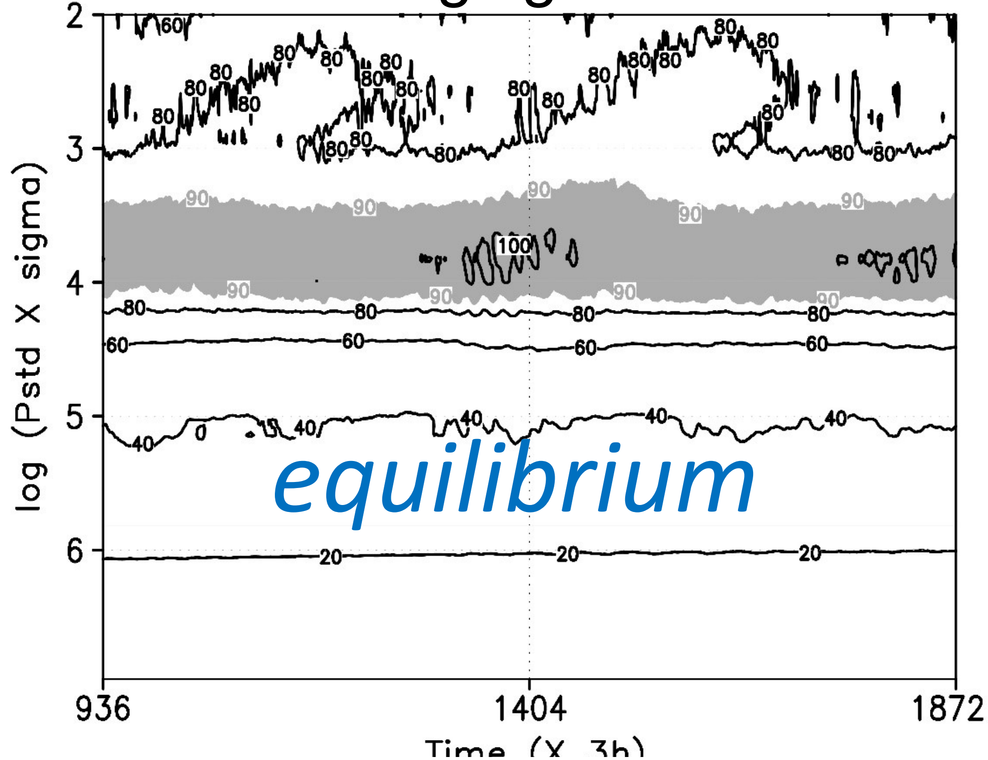

Zonal wind (contour)   Temperature (contour)

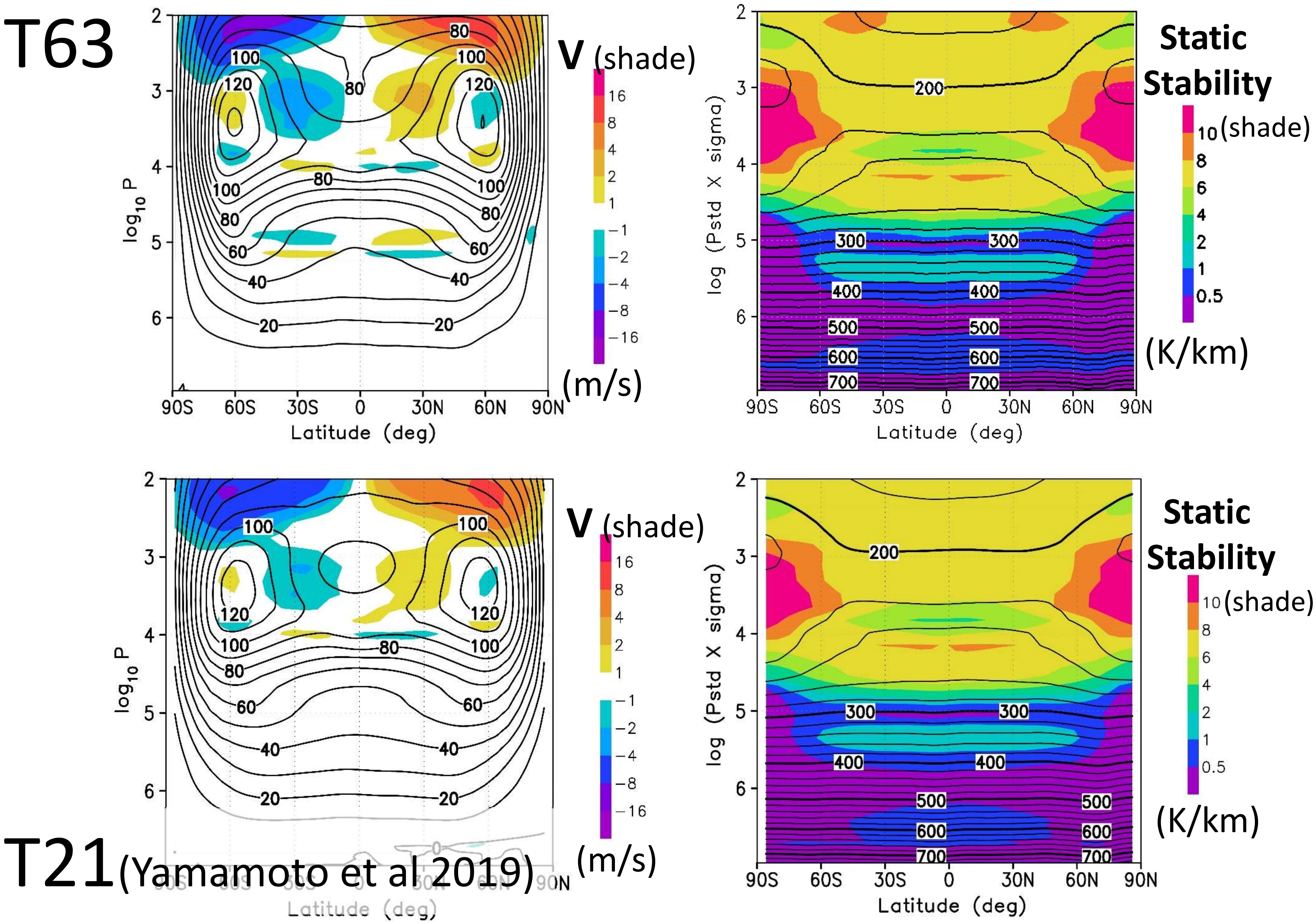

wind, temperature & **radiative heating (bottom)**

T63

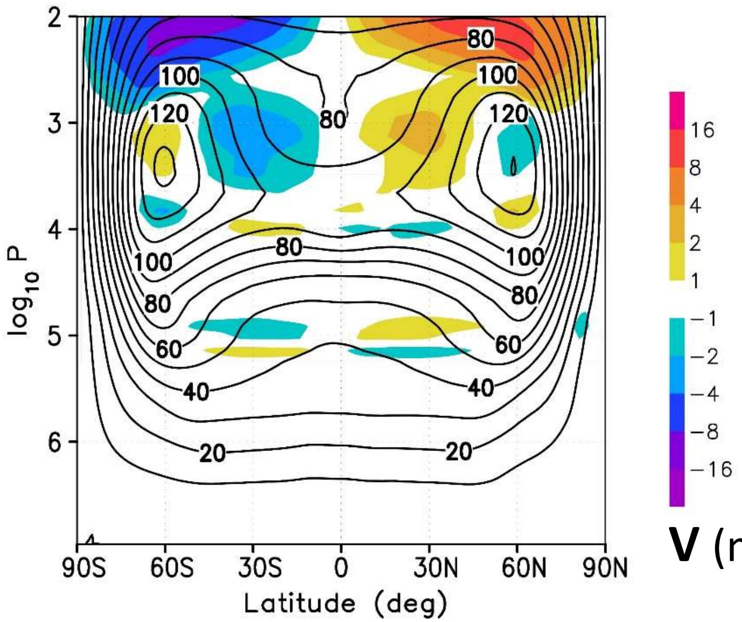

V (m/s)

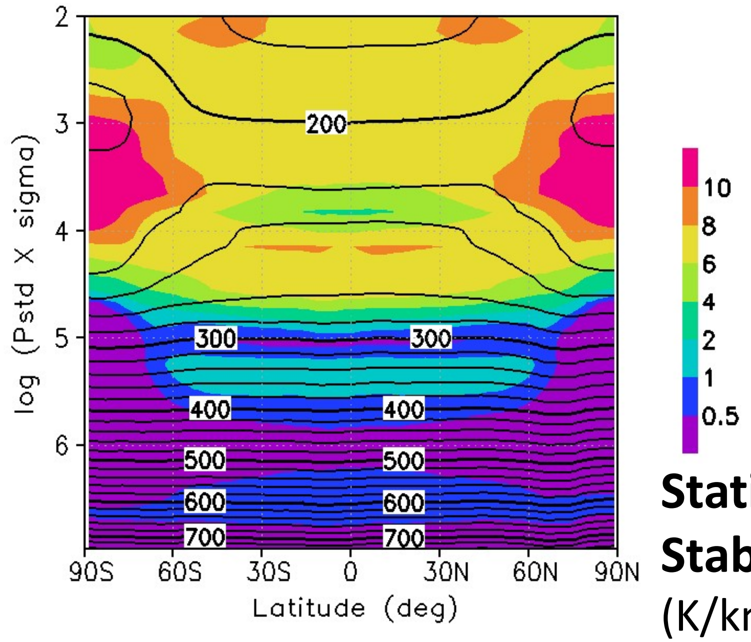

Static Stability (K/km)

Equatorial heating

Polar cooling

E-P Radiative *imbalance*

Local radiative *balance*

Short-wave heating (contour, K/d)

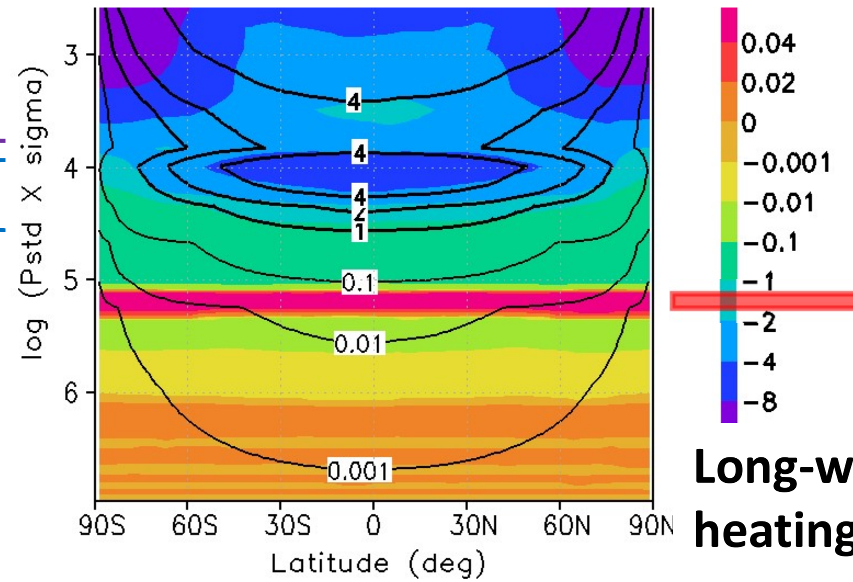

IR heating at the cloud bottom

Long-wave heating (shade, K/d)

wind, temperature & **radiative heating (bottom)**

T63

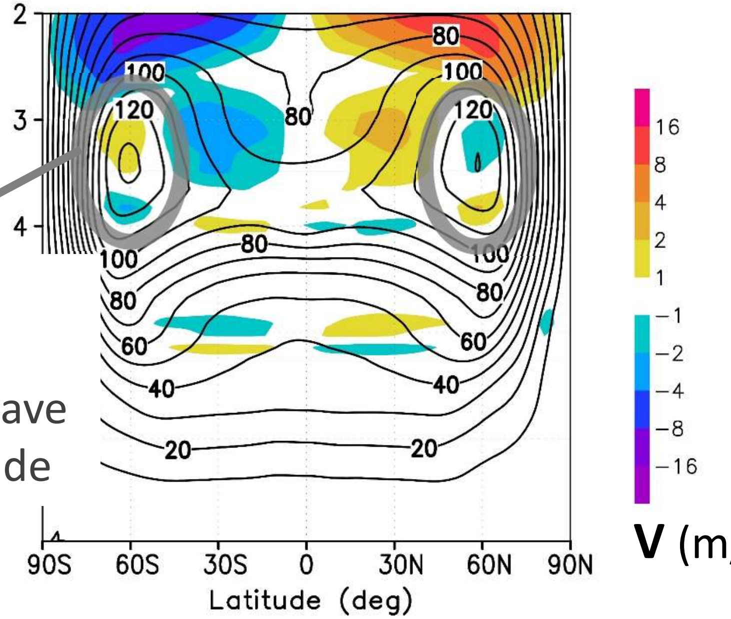

V (m/s)

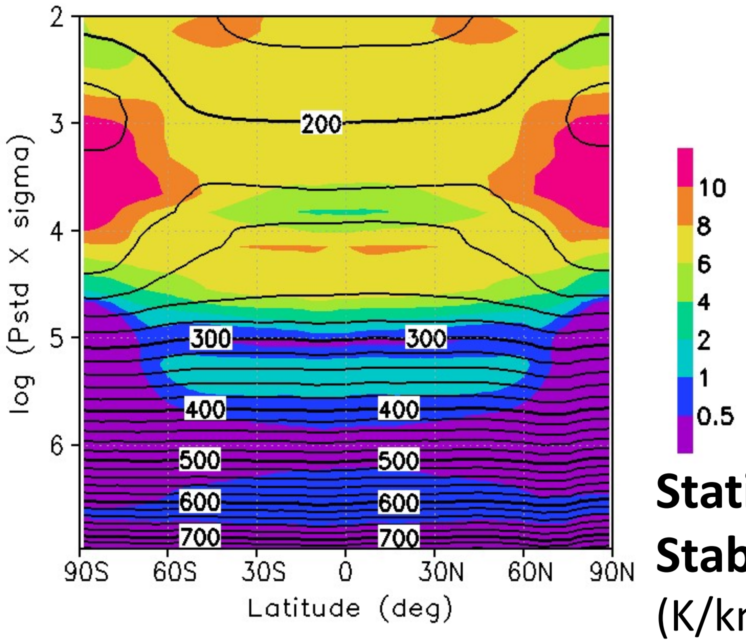

Static Stability (K/km)

Ferrel cell induced by baroclinic wave & thermal tide

***Strong* Hadley cell**

Equatorial heating
Polar cooling

E-P Radiative *imbalance*

Local radiative *balance*

***Weak* meridional flow**

Short-wave heating (contour, K/d)

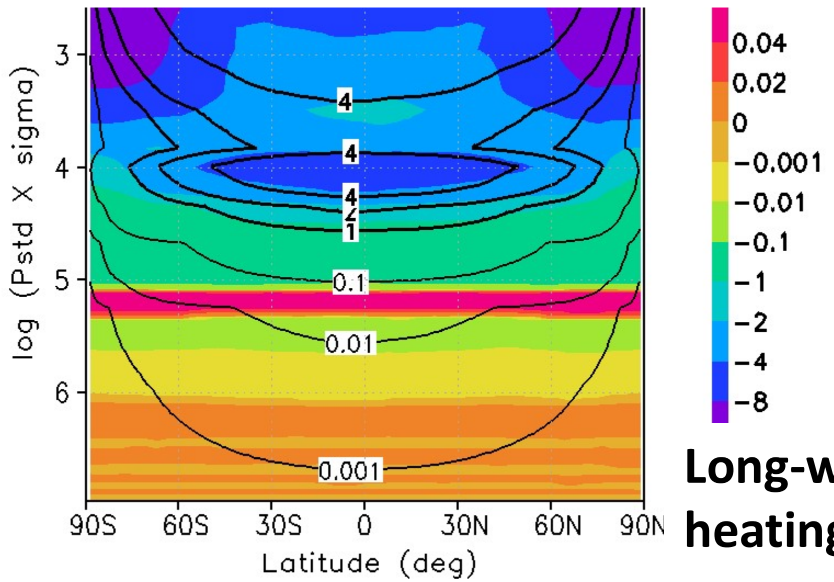

Long-wave heating (shade, K/d)

wind, temperature & **radiative heating (bottom)**

T63

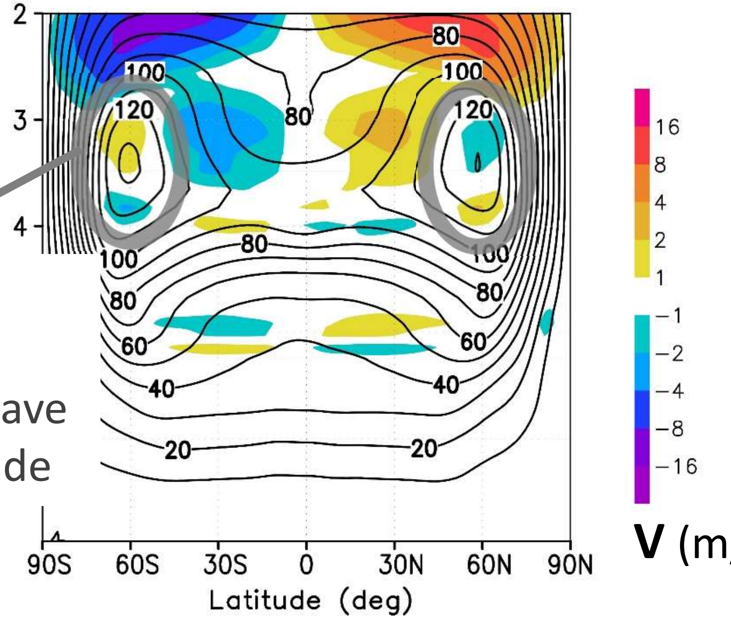

V (m/s)

Ferrel cell
induced by
baroclinic wave
& thermal tide

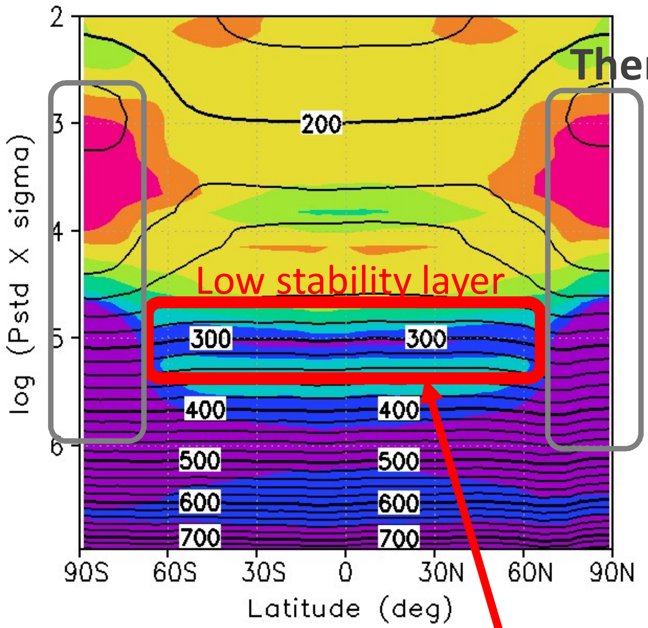

Thermal wind relation

Static Stability (K/km)

***Strong* Hadley cell**

Equatorial heating
Polar cooling

E-P Radiative *imbalance*

Local radiative *balance*

***Weak* Return flow**

Short-wave heating (contour, K/d)

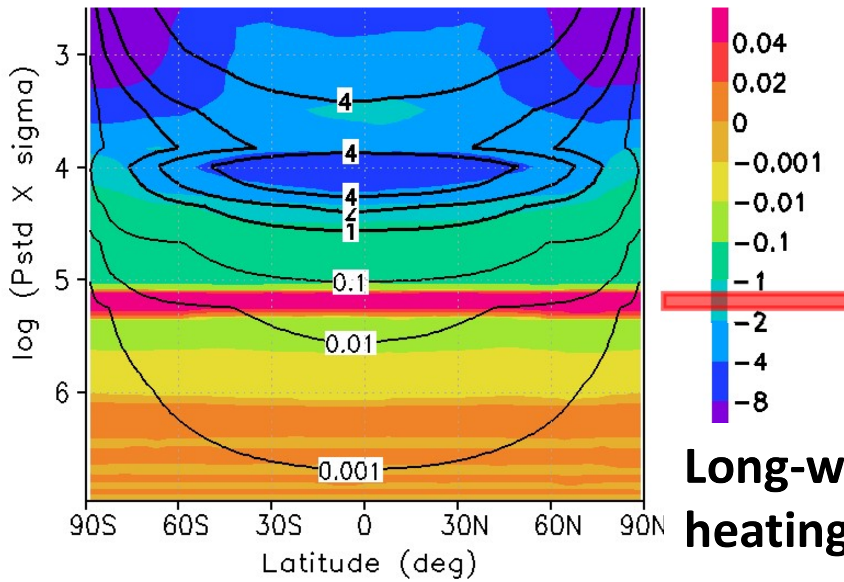

IR heating at the cloud bottom

Long-wave heating (shade, K/d)

U & V with topo

T63

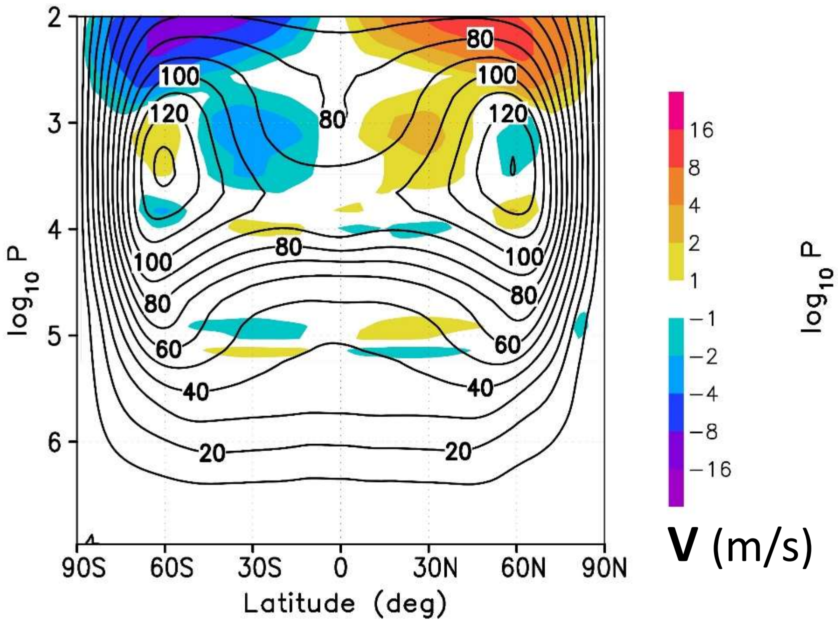

topo–flat

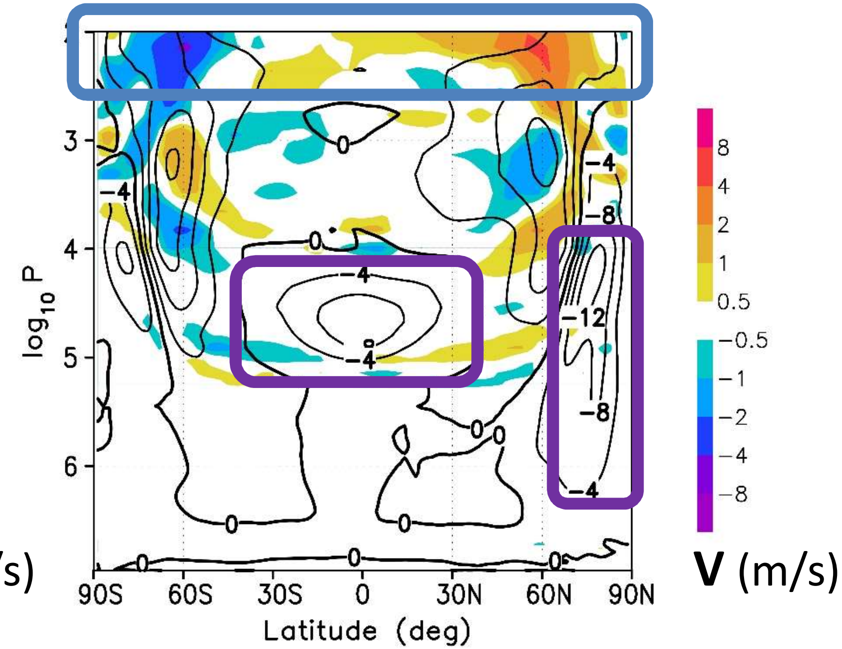

Topographically induced

Zonal wind decrease

Poleward wind enhancement

U & V with topo

T63

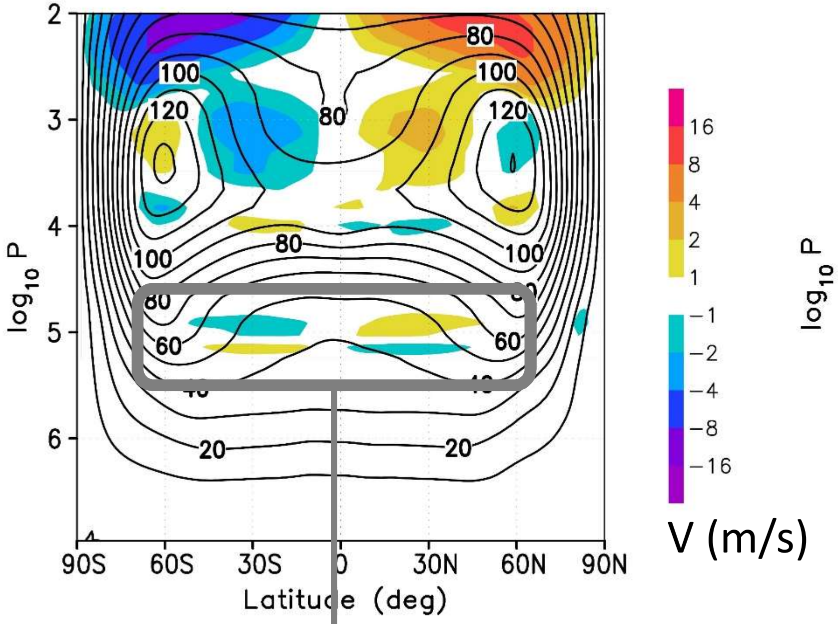

a thin Hadley circulation

topo–flat

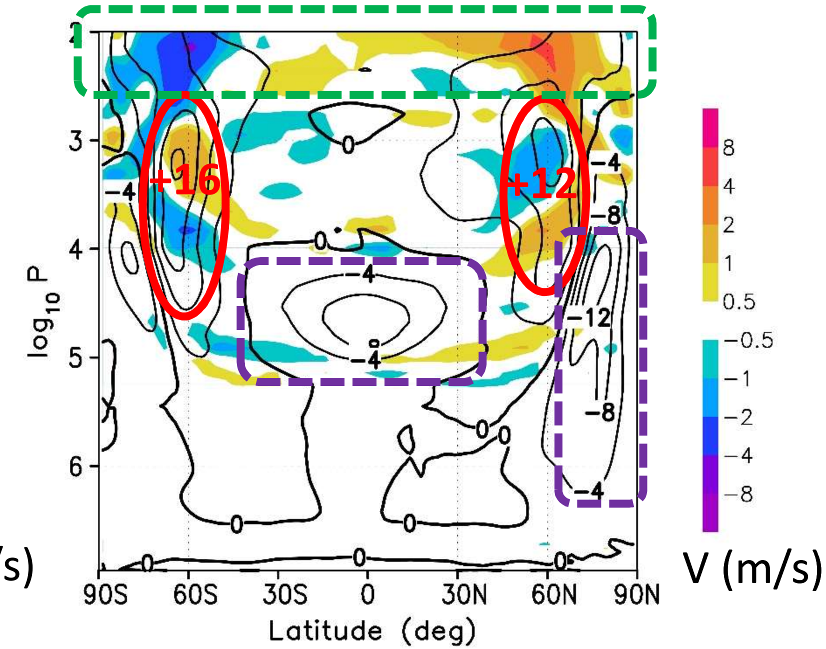

Topographically induced
Zonal wind decrease

Poleward wind enhancement

Enhancements of high-latitude jet and Ferrel circulation

< Note >

These topographical effects are seen in the high-resolution (T63) model

Solar fixed circulation (solar day average)

U (shade) & V (contour)

around the cloud Top (~69.5 km)

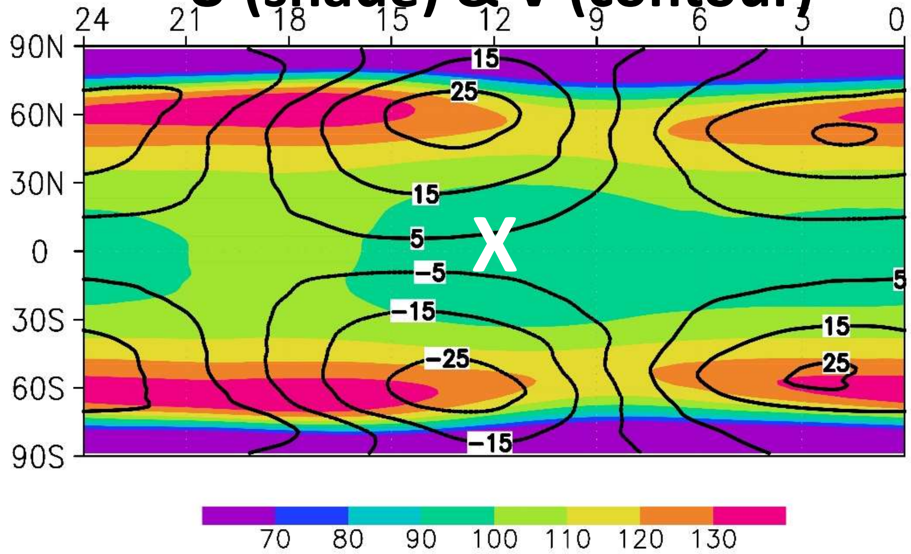

T (shade) & W (contour)

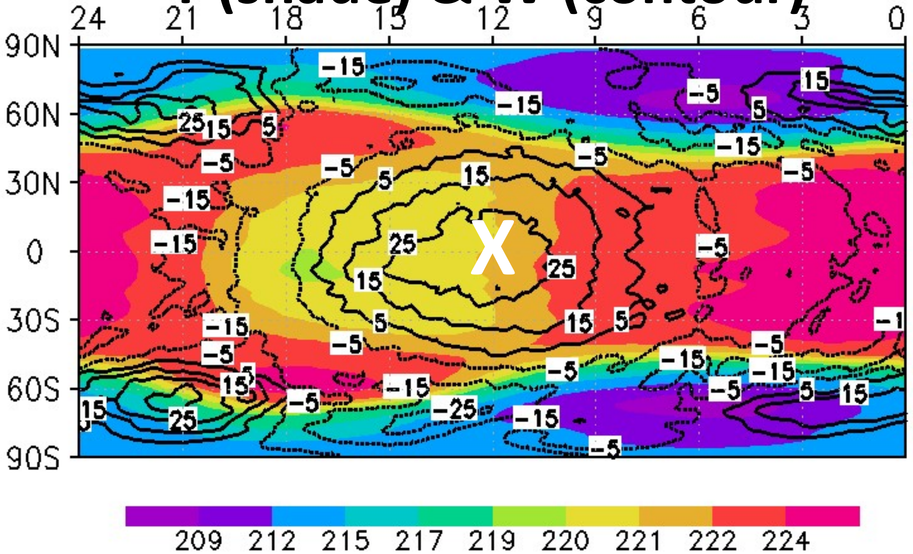

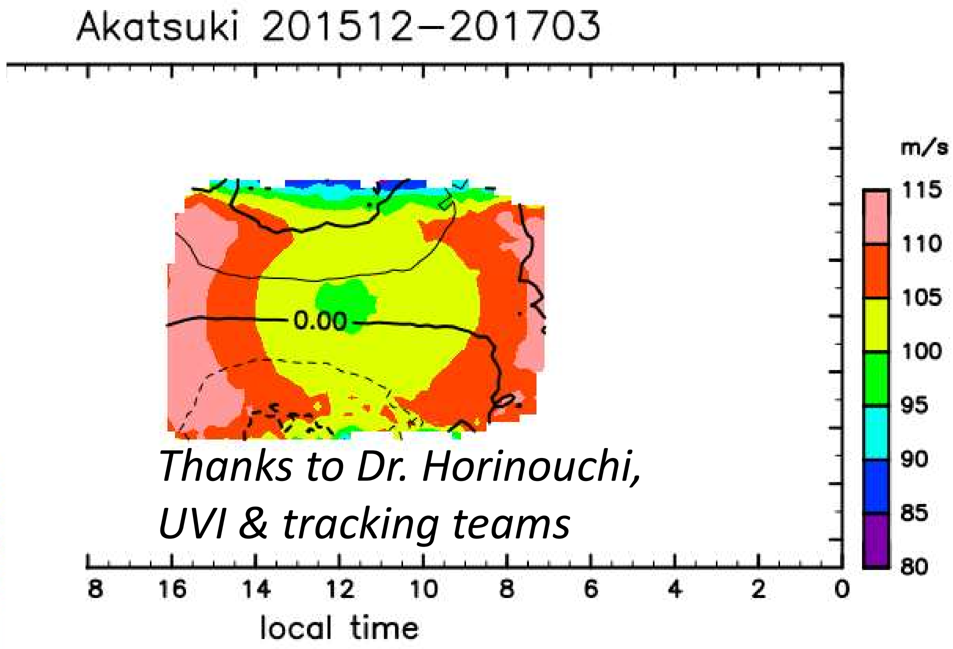

Solar fixed circulation (solar day average)

around the cloud Top (~69.5 km)

U (shade) & V (contour)

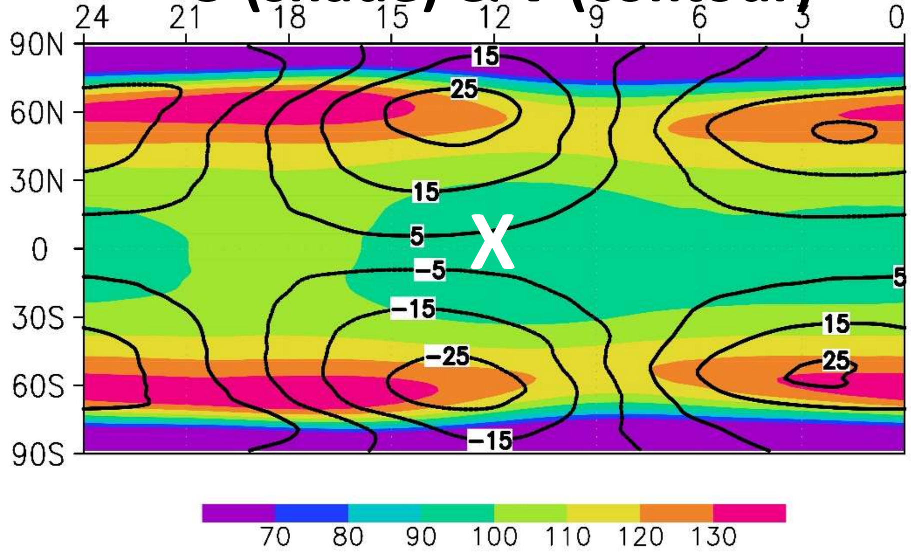

T (shade) & W (contour)

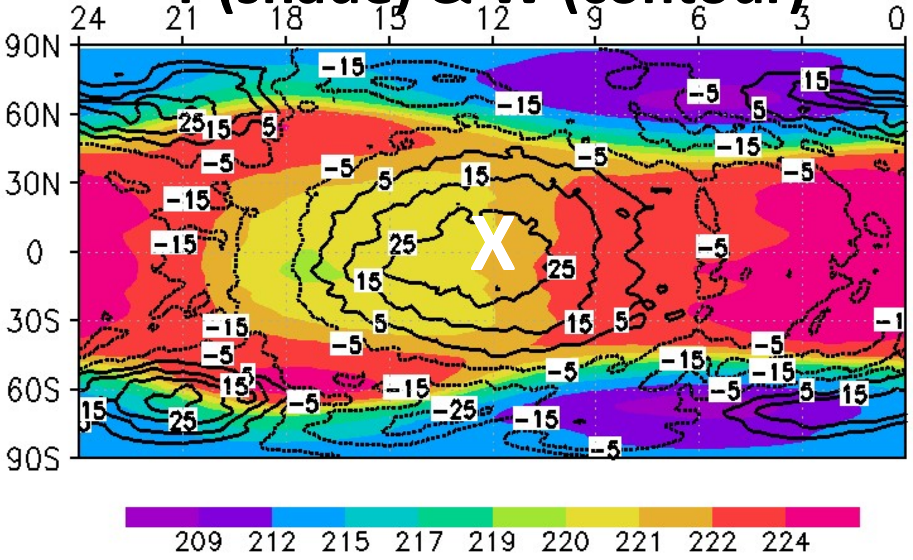

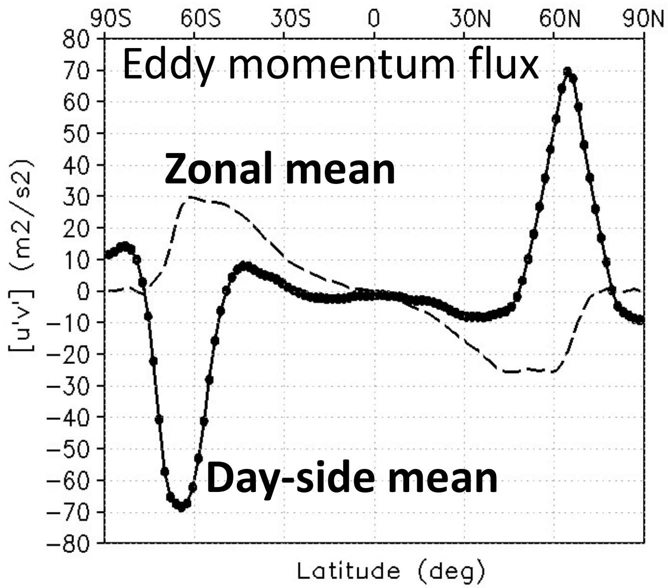

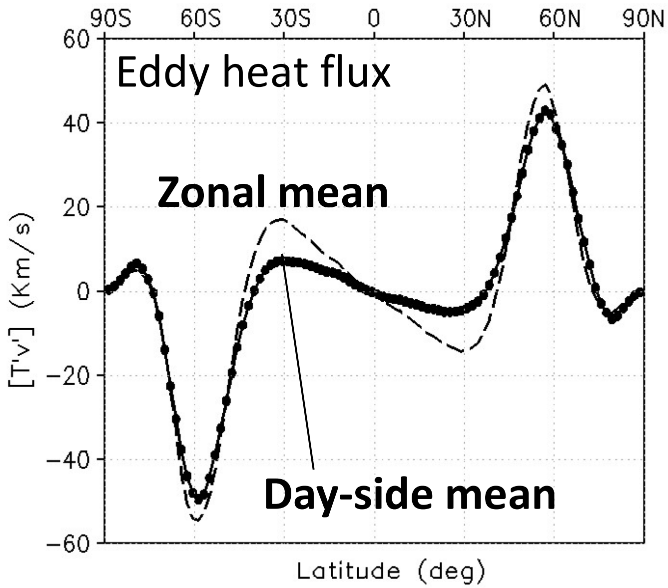

Thermal tide at cloud heating max. (~65.5 km)

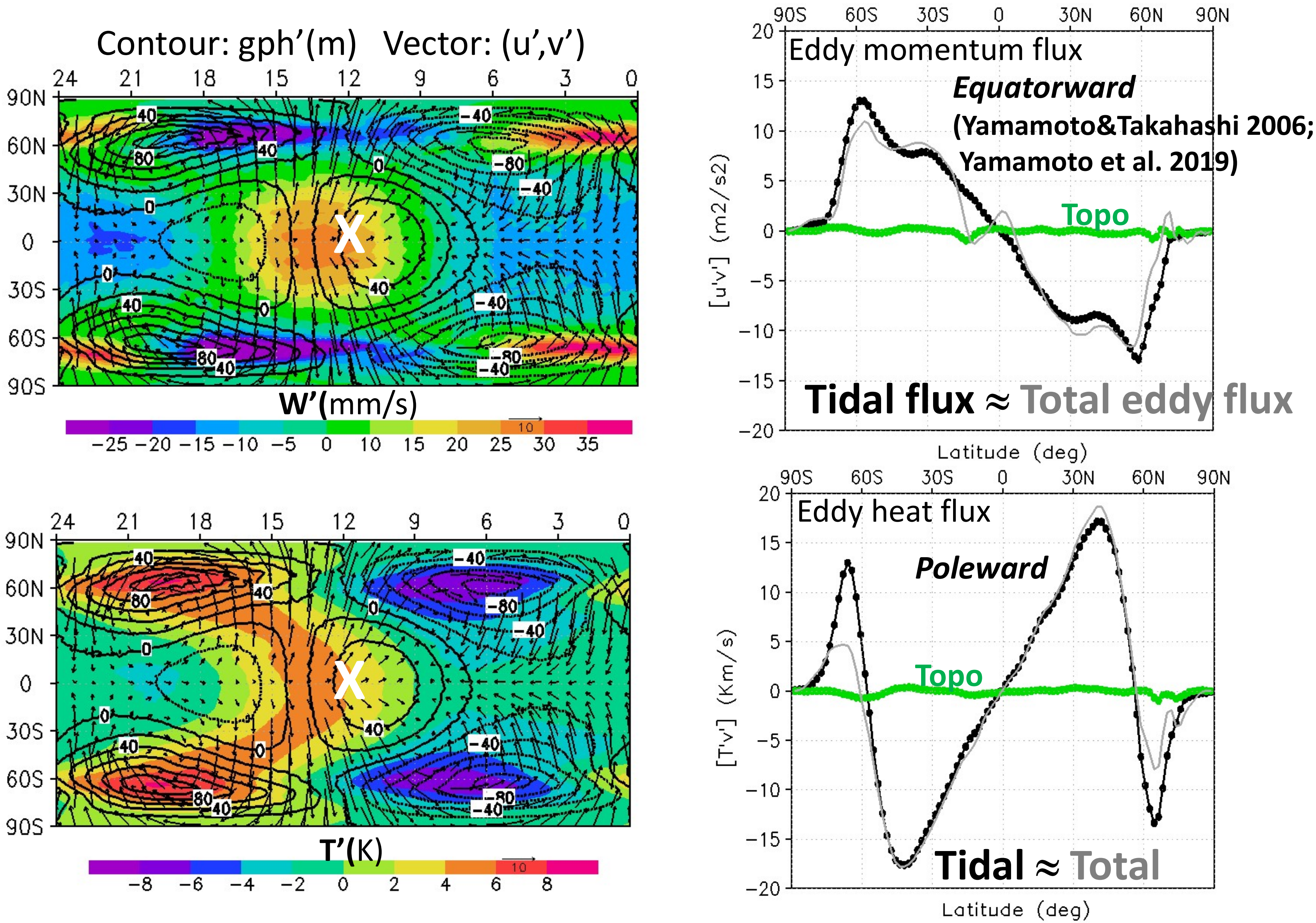

Thermal tide near the equator (~0 deg lat.)

P-weighted T' (contour)

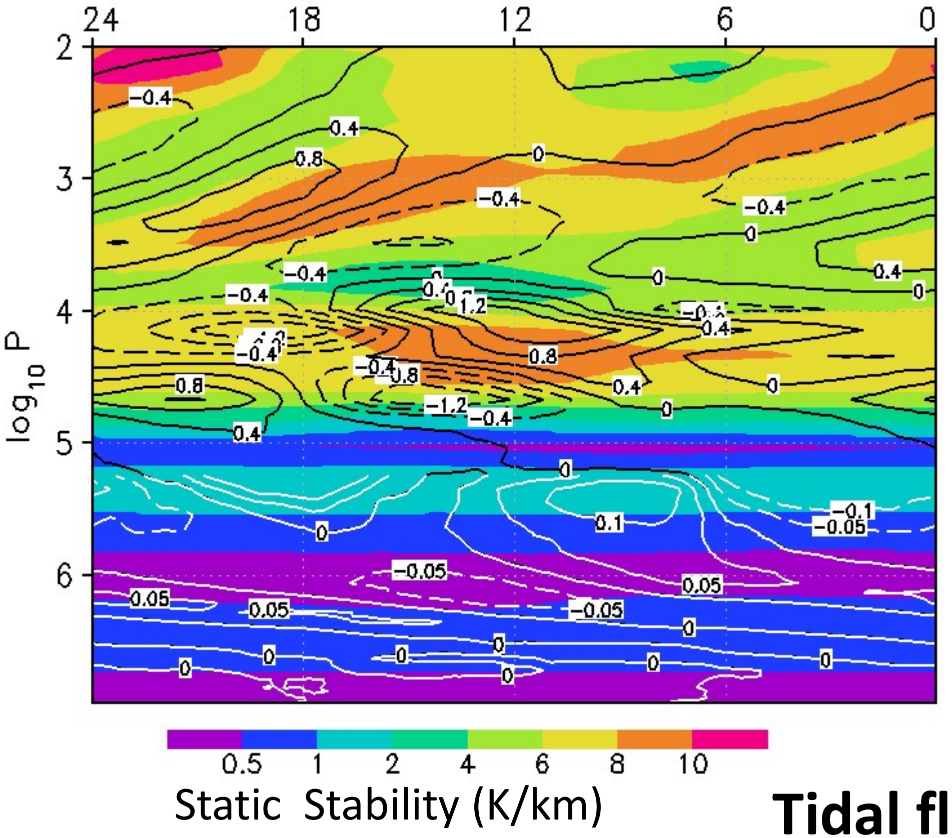

Eddy vertical mom. flux

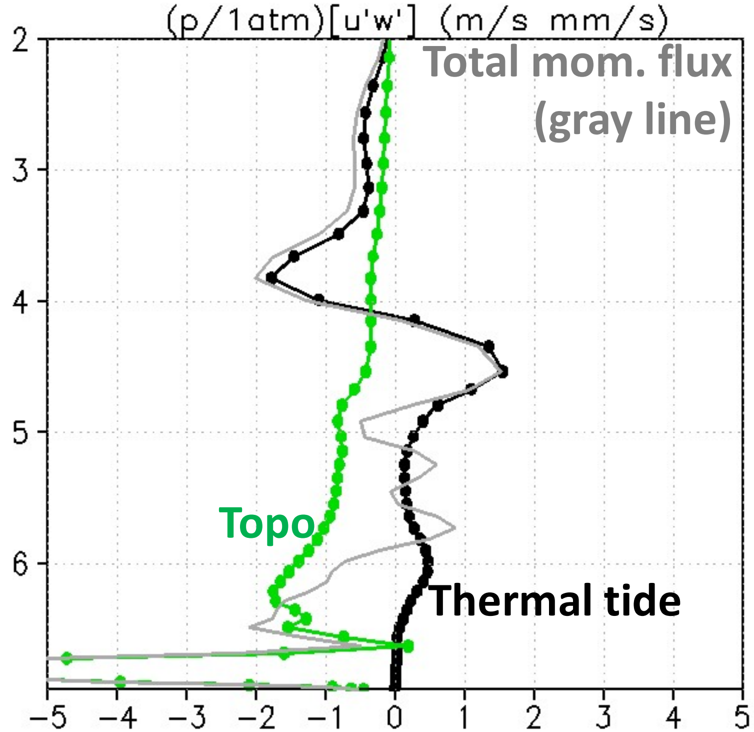

Tidal flux ≈ **Total eddy flux**

in the middle atmosphere

Thermal Tide << Topograph. wave

in the lower atmosphere

Stationary structure (solar-day mean) around 69.5 km

Temperature (shade)

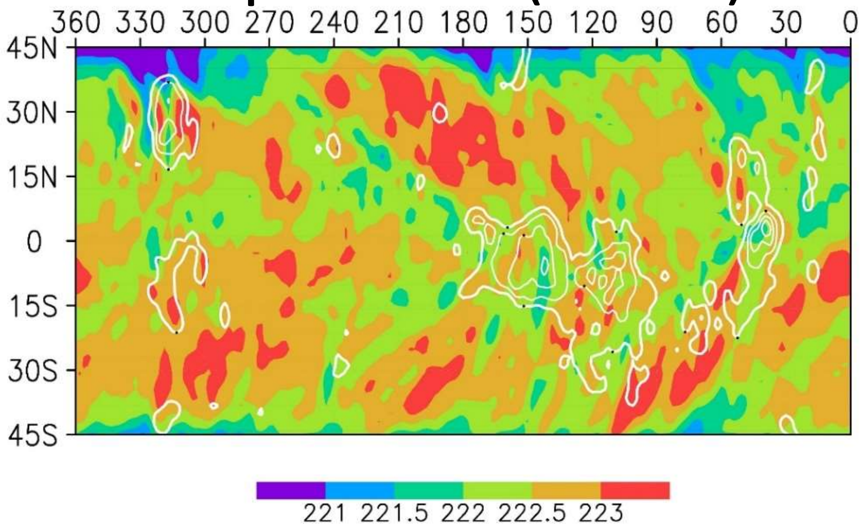

Meridional wind (shade)

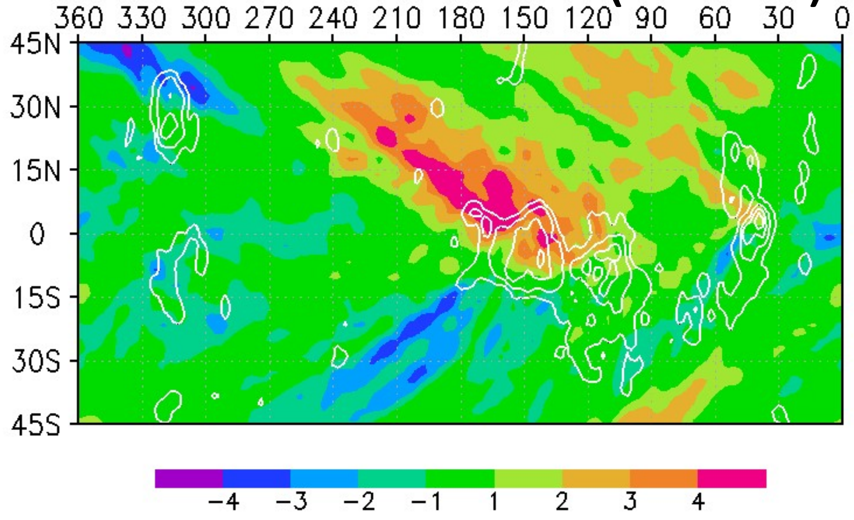

Eddy vertical wind (shade)

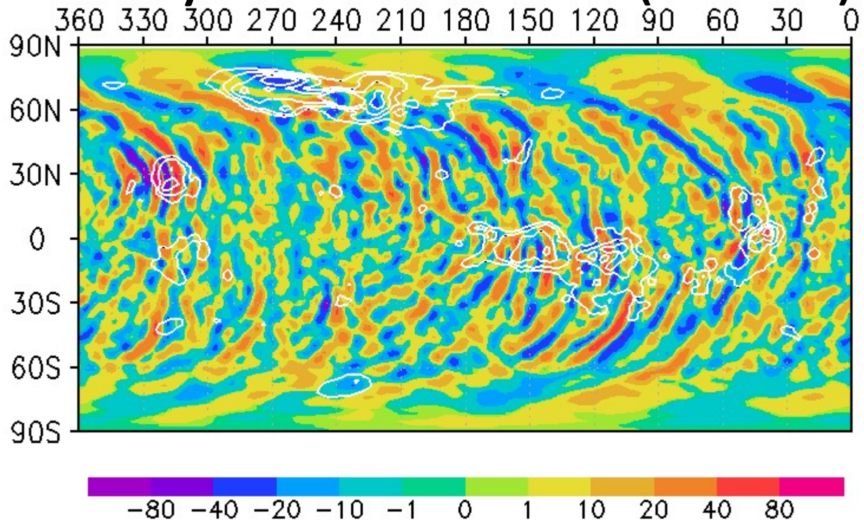

Zonal wind (shade)

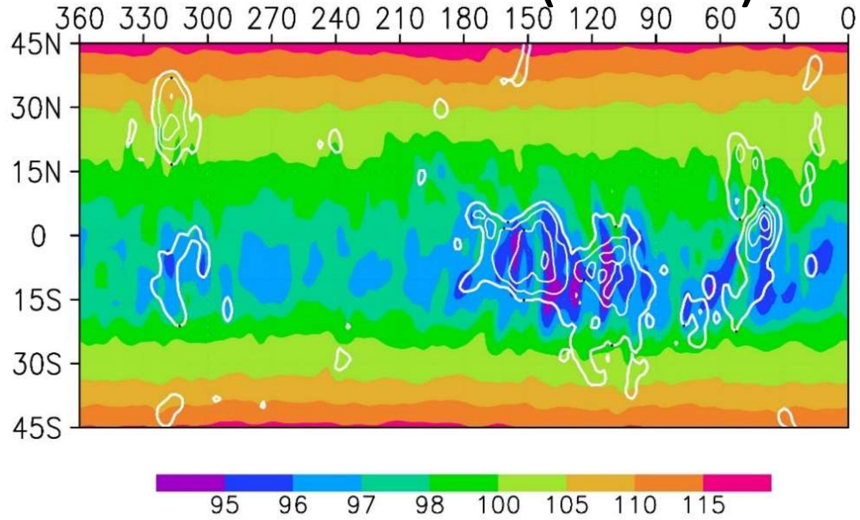

Topographically stationary wave

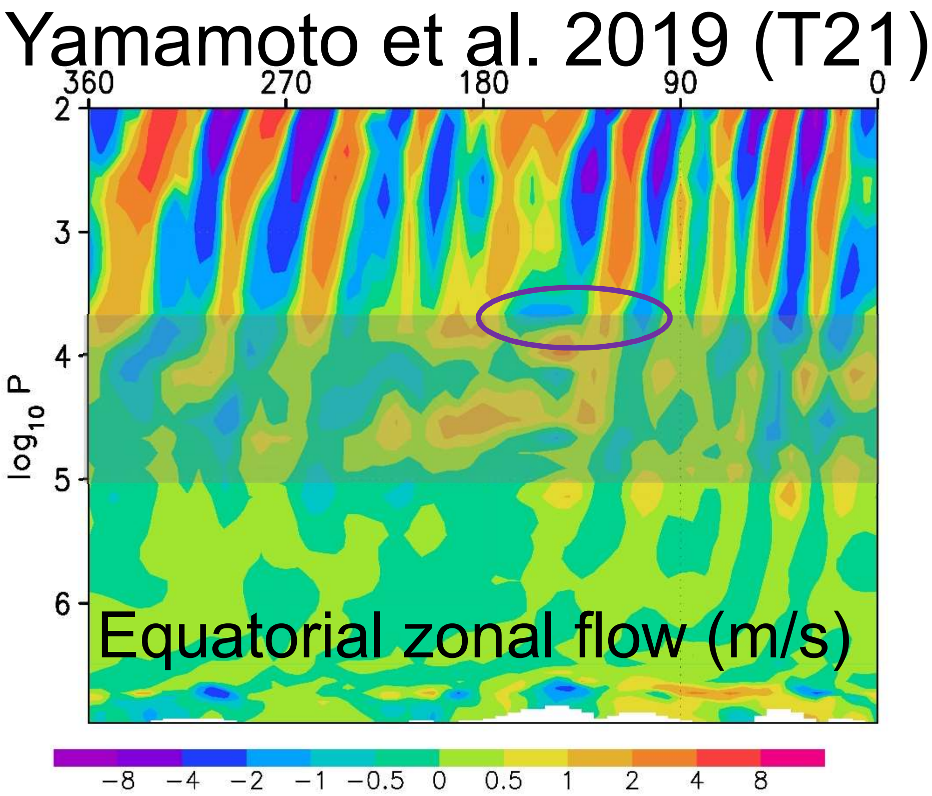

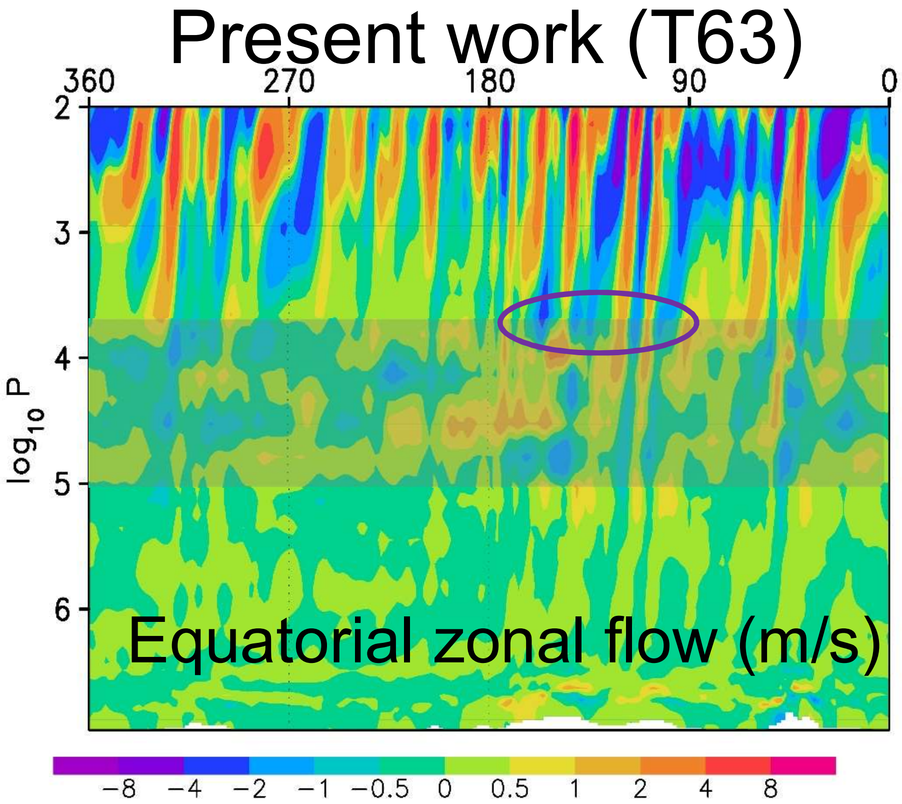

The phase of stationary wave slightly tilts vertically.

The negative phase of the eddy zonal flow forms the local wind decrease at the cloud top over the Aphrodite terra similar to Bertaux et al. (2016).

Summary(1)

- The UV tracked **horizontal flow around the subsolar point** is reproduced .

- **Multi-layered and polar static stabilities** are reproduced.

- **Thermal tides produce *equatorward* momentum flux** (Yamamoto & Takahashi 2006), along with the vertical flux.

- The **zonal-wind decreases at 69 km over Aphrodite Terra**.

- **Day-side mean eddy horizontal fluxes are quite different from the zonal means** owing to meridional flow of the tides.

$\Rightarrow$ These results are the same as the T21 simulation of Yamamoto et al. (2019 Icarus, 321, 232-250).

Summary(2)

Further investigation shows the following results.

- (T63) **Topography weakens cloud-level SR** over the Aphrodite Terra and Maxwell Mt., while it **enhances upper-level poleward flow, zonal jet core and Ferrel circulation.**

- (T63) Topography induces **thin Hadley cell around the cloud base**.

- (T21,T63) **Thermal tides are dominant momentum transporters in the middle atmosphere**, whereas **topographical waves are dominant transporters in the lower atmosphere**.

Future works

- Large- and small-scale cloud features
- Energy and angular momentum budgets